Molecular dynamics simulation of the α-Al_2O_3 lattice: dynamic properties

1998 J. Phys.: Condens. Matter 10 4221

(http://iopscience.iop.org/0953-8984/10/19/010)

J. Phys.: Condens. Matter **10** (1998) 4221–4229. Printed in the UK PII: S0953-8984(98)86168-7

Molecular dynamics simulation of the α-Al_2O_3 lattice: dynamic properties

C Rambaut†, H Jobic‡, H Jaffrezic§, J Kohanoff‖ and S Fayeulle†

† Ecole Centrale de Lyon, Département Matériaux Mécanique Physique, UMR 5621, 36 Avenue Guy de Collongue, 69131 Ecully Cédex, France
‡ Institut de Photocalyse, 69621 Villeurbanne Cédex, France
§ Institut de Physique Nucléaire IN2P3, 69621 Villeurbanne Cédex, France
‖ International Centre of Theoretical Physics, Trieste, Italy

Received 18 July 1997

Abstract. Molecular dynamics simulation of the α-Al_2O_3 crystal was performed. Structural, thermodynamical and vibrational properties were determined by using a modified shell model. In this model, the energy conservation was ensured very accurately by assigning a small mass to each shell and treating them as dynamic variables. Simulation results were compared with experimental data, particularly with inelastic neutron scattering experiments giving the density of phonon states. Calculated structural and thermodynamical properties were in very good agreement with data obtained from the literature. Inelastic neutron scattering experiments were performed; calculated phonon characteristics compared very well with these experimental results.

Introduction

Sapphire or α-Al_2O_3 is a widespread mineral occurring in a variety of high-temperature rock types. Its extreme hardness and resistance as well as its optical properties lead to many physical and technical applications. It is of great importance to the chemical industry as a catalyst. Due to the many applications of α-Al_2O_3 as a structural, electronic and optical material, there is an increasing need to understand its dynamic properties.

Further, as dynamic mechanisms occur in materials in the range of the picosecond to the femtosecond, it is very difficult to observe and analyse them experimentally. So, molecular dynamics simulation can play a valuable role in revealing and interpreting in a easier way the dynamic behaviour of a crystal lattice. The introduction of the shell model by Dick and Overhauser [3] to describe the ionic polarization has given important improvements in the reproduction of dynamic properties of the crystal lattice. Now, it is in current use in simulation [4, 5]. Nevertheless, it presents some drawbacks as regards energy stability in molecular dynamics. In this study, a modified shell model has been developed to ensure simulation to high accuracy. Using this new shell model, some structural, thermodynamical and vibrational properties of α-Al_2O_3 were determined from simulation and compared with experiment.

1. Shell model

Molecular dynamics has been used to simulate the properties of the α-Al_2O_3 lattice. This method has already proved efficient in simulating lattice properties [1, 2]. In order to have a

0953-8984/98/194221+09$19.50

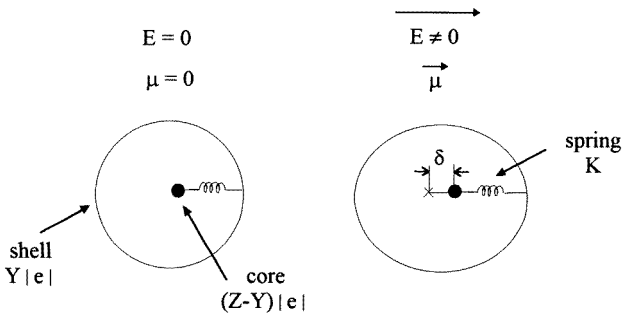

Figure 1. Core–shell model. δ is the displacement of the shell with respect to the core resulting from the polarizing field E.

good representation of the dynamic behaviour, each particle is described using the core–shell model which enables introduction of ionic polarization.

This model was first introduced by Dick and Overhauser [3] and was used in various studies on wide-band oxides [4, 5]. Each ion is represented by a massive core and a massless shell which 'simulates' the polarizable valence electrons. The total ionic charge Z is divided between core and shell and the interaction between the core and the shell of the same ion is described using a harmonic spring model with a force constant K. Polarization is described in terms of the displacement of the shell relative to the core through the polarizing field due to the surrounding ions. The magnitude of the dipole model is determined by the amplitude of the core–shell separation (figure 1). Therefore, in contrast to the rigid model, the strong coupling occurring in ionic solids between the short-range interaction and the polarization is thus taken into account.

This model, however, presents an important drawback: the assumption of the massless shell is a way to introduce the adiabatic approximation (Born–Oppenheimer) [6] and so the shells have to follow instantaneously the motion of the core. This condition is very difficult to obtain in practice. Consequently, due to the partial relaxation of the shells, the motion of the cores is damped during the simulation and a slight inconsistency between force and energy results [7].

We have solved this problem by assigning a small mass to the shells which are now treated as dynamic variables (like the cores) but evolving along their own fictitious equation of motion. By borrowing ideas from the Car–Parinello method [8], the adiabatic condition may be maintained to the necessary degree to give reliable ion dynamics. The equations of motion for the additional degrees of freedom are integrated in parallel with the equations governing the core positions with a short time step, adapted to the rapid oscillations which the additional degrees of freedom undergo, from a starting point at which the adiabatic condition is satisfied. This second order dynamics for the shells gives rise to oscillating fictitious forces on the cores that average out during the slower dynamics of the cores [8, 9]. If the range of oscillation frequencies does not overlap the density of states of the translational degrees of freedom of the system studied, the energy transfer between the translational and the additional degrees of freedom is slow and adiabacity is maintained for long periods [24]. The oscillation frequencies can be tuned into an appropriate range by choosing appropriate values for the mass of the shells. Moreover, the value of the integration time step is also determined by this mass. In practice, the largest mass compatible with a reasonable energy transfer during the typical times of the simulation is chosen to allow the time step to be maximized. The mass of the shells has been chosen to be 10% of the

proton mass. This choice pushes the oscillation frequencies out of the range of the ionic translational oscillations, so ensuring energy conservation to high accuracy.

2. Other details on simulation

The interaction between cores is assumed to be purely Coulombic whereas the interaction between shells has two components: a long-range purely Coulombic interaction and a short-range interaction described by the Buckingham potential [10] as follows:

$$V_{ijB} = A\exp\left(-\frac{r_{ij}}{\rho}\right) + \frac{C}{r_{ij}^6}. \tag{1}$$

The choice of short-range interaction between the shells allows taking into account the strong coupling between short-range repulsion and polarization occurring in ionic solids. Indeed, polarization, which involves displacement of valence shell electrons, modifies the short-range interaction between ions. The omission of this coupling leads to a poor description of dielectric and defect properties [11].

The Coulombic component is calculated under periodic boundary conditions using the Ewald method [12] which allows us to cope with long-range forces. The simulation cell, containing N particles in a volume V, is surrounded on all sides by periodic replications of itself forming an infinite sphere.

Before determining the dynamic properties, each ion was placed so as to assure a correct description of the crystallographic lattice of the studied system, i.e. rhombohedric for α-Al_2O_3. The velocity assigned to each particle was randomly fixed so that the system was set to a pre-determined temperature. Then the system was relaxed toward its equilibrium state at the desired temperature. Simulations were carried out in the canonical system where the number of the particles N, the volume V and the temperature T of the system are kept constant. The relaxation and the realization of the canonical system were obtained by using the Nosé–Hover thermostat method [13]. The Verlet algorithm was employed to update the translation motion of all the species at the end of each time step. A short time step of 0.1 fs was used in the simulation due to the small mass of the shells.

3. α-Al_2O_3 simulation

The sapphire lattice can be described in the hexagonal system as a succession of anionic and cationic planes. The oxygen ions form an hexagonal compact stacking slightly distorted in order to make room for the aluminum ions which occupy two-thirds of the octahedral interstices [14, 15]. The space group is $R\bar{3}c$ belonging to the trigonal system. The α-Al_2O_3 structure is shown in figure 2.

The simulation of the α-Al_2O_3 lattice was performed using the values of the parameters displayed in tables 1 and 2. The spring constants and the partial charges of the shell-model are given in table 1. The parameters A_{ij}, C_{ij} and ρ of the Born–Mayer potential describing the short-range interaction are given in table 2. All values have been taken from [16].

3.1. Structural investigation

The radial distribution functions $g(r)$ for Al^{3+} and O^{2-} were simulated at 300 K. They represent the probability of finding a pair of atoms at a distance r apart, relative to the probability expected for a completely random distribution at the same density [12]. They provide insight into the crystal structure. Figure 3 shows the total radial distribution obtained

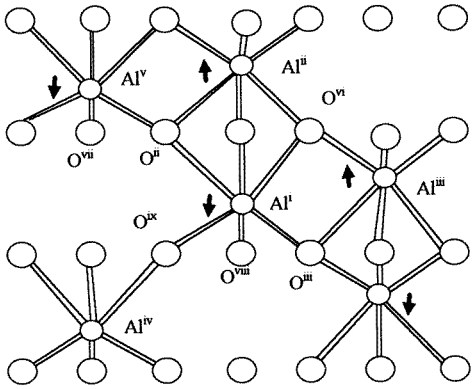

Figure 2. Structure of α-Al_2O_3 projected on $(\bar{1}30)$. The interatomic distances chosen in table 3 are represented as well as the direction of the displacement of the different Al^{3+} ions at 2170 K compared with 300 K.

Table 1. Values of the parameters used in the short-range interactions [16].

Interactions	A_{ij} (eV)	ρ (Å^{-1})	C_{ij} (eV Å^6)
Al–Al	0	0.1	0
O–O	22 764	0.149	27.88
Al–O	1 460.3	0.299	0

Table 2. Values of the parameters used in the shell model [16].

Parameters	Al^{3+}	O^{2-}
Spring constant (eV Å^{-2})	92.829	103.07
Core charge (e)	1.6170	0.8106
Shell charge (e)	1.3830	−2.8106

from the simulation of bulk α-Al_2O_3. For comparison, the static pair distribution for the structure given by Wyckoff [15] is also represented. The excellent agreement between crystallographic data and simulation results indicates that the potentials and the model used in the simulation adequately described the structure of α-Al_2O_3, preserving the initial configuration of atoms in the molecular dynamics simulations. Furthermore, the crystal structure of α-Al_2O_3 calculated by molecular dynamics simulation was compared with x-ray studies at $T = 300$ K and $T = 2170$ K [17]. Results are displayed in table 3. Interest was focused on the selected interatomic distances and bond angles represented in figure 3.

It can be seen that simulation results agreed well with the x-ray experimental observations, particularly at 300 K. The calculated interatomic distances shifted from those obtained by x-ray experiment by a maximum deviation of only 2% at 300 K. Moreover, the bond angles exhibited a 5% average deviation at 300 K. At 2170 K, greater differences between simulation and experiment have been observed. These deviations are due to the empirical nature of the potential, as the different parameters of the potential and the shell model were obtained from fitting of experimental data in equilibrium condition.

The displacement of the different Al^{3+} ions depicted in figure 2 revealed that the Al

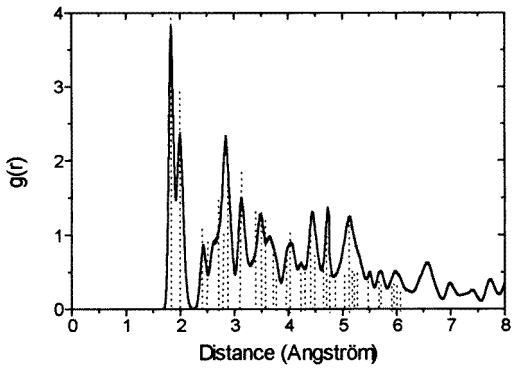

Figure 3. Total radial distribution function of sapphire obtained from simulation (solid line) and from the x-ray diffraction studies of Wyckoff [15] (dotted line).

Table 3. Selected interatomic distances (Å) and bond angles (°) at $T = 300$ K and $T = 2170$ K obtained using simulation and by x-ray diffraction [17].

	Simulation		Experiment	
Distances	300 K	2170 K	300 K	2170 K
Al^{i}–O^{ii}	1.977	2.037	1.971	2.024
Al^{i}–O^{ix}	1.855	1.882	1.852	1.880
Al^{i}–Al^{ii}	2.71	2.802	2.657	2.744
Al^{i}–Al^{iii}	2.77	2.835	2.789	2.847
Al^{i}–Al^{iv}	3.149	3.21	3.214	3.262
Al^{i}–Al^{v}	3.504	3.58	3.496	3.565
O^{ii}–O^{vi}	2.538	2.588	2.522	2.577
O^{ii}–O^{vii}	2.841	2.88	2.863	2.913
O^{ii}–O^{viii}	2.565	2.63	2.619	2.675
O^{ii}–O^{ix}	2.67	2.725	2.724	2.779
Al^{i}–O^{ii}–Al^{ii}	91.27	91.67	84.76	85.35
Al^{i}–O^{vi}–Al^{iii}	94.32	84.85	93.61	93.58
Al^{i}–O^{ix}–Al^{iv}	119.91	121.99	120.38	120.41
Al^{i}–O^{ii}–Al^{v}	131.86	130.66	132.19	131.95
O^{ii}–Al^{i}–O^{vi}	78.35	77.87	79.53	79.09
O^{ii}–Al^{i}–O^{ix}	87.21	87.46	86.40	86.42
O^{ix}–Al^{i}–O^{iii}	102.40	103.03	101.20	101.57
O^{ii}–Al^{i}–O^{iii}	162.05	161.18	164.13	163.57

move toward the vacant octahedral site on the threefold axis. As was shown above, the Al^{i}–Al^{ii} bond, which is parallel to the *c* axis, is the shortest of all the Al–Al distances in the structure and increases dramatically from 2.77 Å at 300 K to 2.835 Å at 2170 K. Therefore, the thermal expansion of this distance is obviously the greatest of all the Al–Al distances which fall in the following order: distances across faces, distances across edges and distances across corners. This involves the increasing of the uniformity of the Al–Al distance between neighbouring Al^{3+} at high temperature.

The displacement of the O^{2-} ions is less obvious than that of the Al^{3+} ions. But the changes in the position of the O lead to less distorted close-packed planes of O atoms at high temperature.

3.2. Vibrational properties: phonon density

According to linear response theory, the phonon density can be obtained from the velocity autocorrelation function [18]. Thus the density of phonon states $\rho(\nu)$ is taken to be the Fourier transform of this autocorrelation function:

$$\rho(\nu) \propto \int_0^\infty \frac{\langle V(0)V(t)\rangle}{\langle V(0)^2\rangle} \cos(2\pi\nu t)\,\mathrm{d}t \tag{2}$$

where $V(t)$ is the velocity of an atom computed at the end of each time step (every 0.1 fs) using the Verlet algorithm. The velocity autocorrelation function is assumed to be real and $\rho(\nu)$ is normalized according to

$$\int_0^\infty \rho(\nu)\,\mathrm{d}\nu = 3N \tag{3}$$

where N is the total number of aluminum and oxygen ions in the simulation box [12]. The density of acoustic and optical phonon states has been investigated along the Γ–Z direction in the reciprocal space, the primitive cell of which is shown in figure 4.

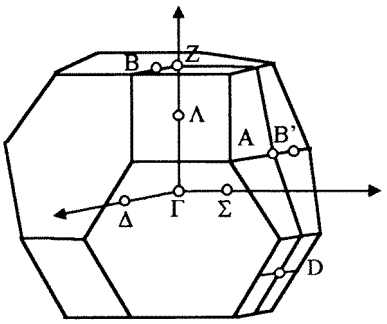

Figure 4. Brillouin zone of sapphire [19].

The density of phonon states was measured by inelastic neutron scattering (INS) experiments performed at the Laue–Langevin Institute in Grenoble. The specimen was a transparent α-Al_2O_3 single crystal grown by the Verneuil method. It was annealed at 1500 °C for 4 hours and then cooled to 20 K, the temperature at which the INS experiments were carried out, in order to reduce the multiphonon background.

Figure 5 shows the results obtained using simulation and experimentation. The simulation compared well with experiment. Although only an idealistic material containing perfect ions interacting through a potential was considered, the model gave good results in reproducing the dynamical properties of α-Al_2O_3. The optical vibrations associated with the atomic displacements had a maximum frequency of 27 THz.

3.3. Thermodynamic properties

The energy created by the vibration resulting from the oscillation of the atoms around their equilibrium position determines some thermodynamic properties such as the temperature, heat capacity, entropy and electrical resistivity which characterize the dynamic behaviour of the lattice.

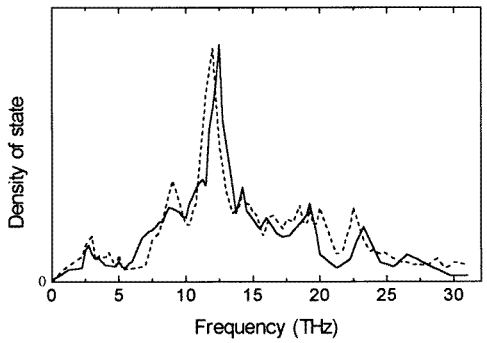

Figure 5. Density of states ρ versus the frequency ν calculated by simulation (solid line) and obtained by inelastic neutron diffusion experiment (dashed line) at 20 K.

The calculated density of phonon states $\rho(\nu)$ at 20 K can be used to derive the heat capacity C_v which is given for quantum harmonic oscillators [19] as follows:

$$C_v(T) = \frac{1}{k_B}\int_0^{\nu_{\max}} \left(\frac{h\nu}{\exp(h\nu/k_BT)-1}\right)^2 \frac{\exp(h\nu/k_BT)}{T^2}\rho(\nu)\,\mathrm{d}\nu \tag{4}$$

where k_B is the Boltzmann constant, ν_{max} the highest frequency recorded in the $\rho(\nu)$ spectrum, h the Planck constant and T the temperature. $\rho(\nu)$ is assumed not to change significantly with temperature, so one simulation at a given temperature is sufficient to obtain C_v (at virtually any other temperature). The harmonic approximation is valid as long as the atomic displacements remain small, a condition verified primarily at low temperature.

The heat capacity in a molecular dynamics simulation can be calculated in another way using the fluctuations in the total energy of the system E [12, 20].

$$C_v(T) = \frac{\left[\langle E^2\rangle - \langle E\rangle^2\right]}{k_BT^2} \tag{5}$$

but it is valid only for classical particles in a canonical system. For this reason, the equation (5) can only be applied at high temperatures. It gives meaningful values of C_v only for temperature superior to the Debye temperature θ_D. In evaluating $C_v(T)$, it is also necessary to perform different simulations to obtain variations of the kinetic energy at different temperatures.

To compare with experimental data which are usually obtained at constant pressure, C_p is calculated from the theoretical C_v by the following relation

$$C_p(T) = C_v(T) + \frac{\beta^2 vT}{\kappa_T} \tag{6}$$

where v is the volume of the system, β the coefficient of volume expansion and κ_T the isothermal compressibility. These parameters are taken from experimental data [21, 22].

The difference between C_v and C_p is usually small in solids. This is the case in α-Al_2O_3 sapphire, as represented in figure 6 where theoretical C_v and C_p are compared with experimental values of C_p at different temperatures [23]. According to the temperature, the theoretical values of C_v were calculated using the equations (4) or (5). For a classical harmonic system, C_v is simply $3R$ according to the Dulong–Petit law. Using the Lebowitz equation (5) (where no harmonic approximation is assumed) a value slightly smaller than $3R$ was also found at 1000 K. But at very low temperature, C_v remained closer to $3R$ as

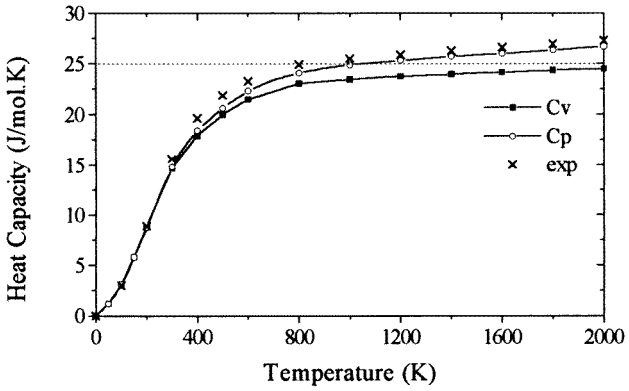

Figure 6. Comparison between theoretical heat capacity at constant volume C_v and at constant pressure C_p obtained from the equations (4) or (5) and (6) and experimental values [23].

the quantum effects were not taken into account. The theoretical results are very similar to the experimental values. However, at high temperature C_p is expected to be larger than C_v.

4. Conclusion

In this study, a new shell model which ensures energy conservation to high accuracy was employed to reproduce the α-Al_2O_3 crystal behaviour. In opposition to the earlier shell model, a small mass was assigned to each shell; these were now treated as dynamic variables.

Good agreement between experiment and calculations was demonstrated for structural, thermodynamical and vibrational properties of α-Al_2O_3. In particular, at 300 K, the total radial distribution function as well as the different interatomic distances and bond angles in α-Al_2O_3 were well reproduced by molecular dynamics simulations. At very high temperature, due to the empirical nature of the potential, deviations appeared. The density of phonon states obtained by simulation compared well with inelastic neutron scattering experiments. Thus, the use of such a modified shell model is validated by experiment. Due to its important applications and its structural complexity, α-Al_2O_3 was a good material to test the validity of our model and molecular dynamics a good tool to obtain meaningful information on its behaviour.

It could be also interesting to compare our results obtained using such a modified but simple shell model with those that would be given by a more complex model, such as the compressible ion model with dipole and quadrupole anion polarizabilities (CIM–DQ) [25]. This semi-empirical model, developed by Wilson *et al*, proved to be very efficient in calculating energetic and static properties. In contrast to the shell model, it was successful in predicting the stability of the α-Al_2O_3 structure with respect to the bixbyite structure by accounting for the induction energy associated with the formation of both anion-induced dipoles and quadrupoles [25]. Nevertheless, this model is based on a polarizable point ion model which previously failed in reproducing dynamic properties.

References

[1] Lindan P J D and Gillan M J 1994 *Phil. Mag.* B **69** 535
[2] Wilson M, Madden P A, Pyper N C and Harding J H 1996 *J. Chem. Phys.* **104** 8068–81

[3] Dick B G and Overhauser A W 1958 *Phys. Rev.* **112** 90
[4] Shluger A L, Rohl A L, Gay D H and Williams R T 1994 *J. Phys.: Condens. Matter* **6** 1825–46
[5] Jacobs P W M and Kotomin E A 1993 *Phil. Mag.* A **68** 695–709
[6] Ashcroft N W and Mermin N D 1976 *Solid State Physics* int. edn (Philadelphia, PA: Saunders)
[7] Dixon M and Sangster M J L 1976 *J. Phys. C: Solid State Phys* **9** 909
Remler D K and Madden P A 1990 *Mol. Phys.* **70** 921
[8] Car R and Parrinello M 1985 *Phys. Rev. Lett.* **55** 2471
[9] Rambaut C, Oh K H, Jaffrezic H, Kohanoff J and Fayeulle S 1997 *J. Appl. Phys.* **81** 3263–7
[10] Harding J H 1991 *Computer Simulation in Materials Science (NATO ASI Series E205)* ed M Meyer and V Pontikis (Dordrecht: Kluwer) p 137
[11] Stoneham A M, Harding J H and Harker T 1996 *MRS Bull.* **21** 29
[12] Allen M M and Tildesley D J 1987 *Computer Simulation of Liquids* (Oxford: Oxford University Press) pp 140–66
[13] Nosé S 1991 *Computer Simulation in Materials Science (NATO ASI Series E205)* ed M Meyer and V Pontkis (Dordrecht: Kluwer) p 21
Evans D J and Holian B L 1985 *J. Chem. Phys.* **83** 4069
[14] Geshwind S and Remeika J P 1961 *Phys. Rev.* **122** 757
[15] Wyckoff R W G 1963 *Crystal Structures* 2nd edn (New York: Interscience)
[16] Catlow C R A, James R, Mackrodt W C and Stewart R F 1982 *Phys. Rev.* B **25** 1006
[17] Ishizawa N, Miyata T, Minato I, Marumo F and Iwai S 1980 *Acta Crystallogr.* B **36** 228–30
[18] Kittel C 1986 *Introduction to Solid State Physics* (New York: Wiley)
[19] Koster G F 1957 *Solid State Physics* vol 5 (New York: Academic) p 173
[20] Lebowitz J L, Percus J K and Verlet L 1967 *Phys. Rev.* **153** 250
[21] May G J and Henderson C M B 1979 *J. Mater. Sci.* **14** 1229
[22] Lewis G K and Drickamer H G 1966 *J. Chem. Phys.* **45** 224
[23] 1985 *J. Phys. Chem. Ref. Data* **14** (Supplement 1) 156
[24] Pastore G, Smargiassi E and Buda F 1991 *Phys. Rev.* A **44** 6334
[25] Wilson M, Exner M, Huang Yin-Min and Finnis M W 1996 *Phys. Rev.* B **54** 15 683